Railway Wheel Flat and Rail Surface Defect Modelling and Analysis by Time-Frequency Techniques

B. Liang, S.D. Iwnicki, Y. Zhao and D. Crosbee

School of Computing and Engineering, Huddersfield University, Huddersfield HD1 3DH, UK

Abstract

Damage to the surface of railway wheels and rails commonly occurs in most railways. If not detected, it can result in rapid deterioration and possible failure of rolling stock and infrastructure components causing higher maintenance costs. This paper presents an investigation into the modelling and simulation of wheel flat and rail surface defects. A simplified mathematical model was developed and a series of experiments were carried out on a roller rig. Time-frequency analysis is a useful tool for identifying the content of a signal in the frequency domain without losing information about its time domain characteristics. Because of this it is widely used for dynamic system analysis and condition monitoring and has been used in this paper for the detection of wheel flats and rail surface defects. Three commonly used time-frequency analysis techniques: Short-Time-Fourier-Transform (STFT); Wigner-Ville Transform (WVT) and Wavelet Transform (WT) were investigated in this work.

Key works: railway, wheelset, vibration analysis, acoustic analysis, time-frequency analysis

1. Introduction

With the recent significant increases of train speed and axle load, forces on both vehicle and track due to wheel flats or rail surface defects has increased and critical defect sizes at which action must be taken have been reduced. This increases the importance of early detection and rectification of these faults. Partly as a result of this, dynamic interaction between the vehicle, the wheel and the rail has been the subject of extensive research in recent years. Wu and Thompson [1] suggested a simplified dynamic model of wheel and rail, which was used for prediction of the wheel and rail impact force and noise in the frequency domain. Pieringer et al [2] developed a fast time domain model for wheel and rail interaction. In this research, rail and wheel are described as linear systems using impulse-response functions. The model enables the calculation of the vertical contact force generated by the small scale roughness of the rail and wheel. Mazilu [3] presented a numerical model to predict the wheel/rail dynamic interaction occurring due to wheel flats. His model treated the rail as an infinite Euler beam supported on a continuous foundation with two elastic layers representing the subgrade. The vehicle is represented by a simplified model consisting of two elastically connected masses and non-linear Hertzian wheel/rail contact is considered. Newton and Clark [4] used a more complex model with the aim of studying the wheel flat and rail impact forces. In their work non-linear elastic Hertzian wheel and rail contact is modelled through an elastic element placed between the wheel and the rail. Belotti et al [5] presented a method of wheel flat detection using a wavelet transform method. In their study, a series of accelerometers were put under the rail bed to detect the impact force caused by a wheel flat and the signals were analysed based on the wavelet property of variable time-frequency resolution. It is claimed that the method is able to detect and to quantify the wheel-flat defect of a test train travelling at different speeds. Jia and Dhanasekar[6] carried out similar research to detect wheel flats using a wavelet approach. However both researchers only used wavelet decomposition of the vibration signals and did not carry out wavelet spectrum analysis of the vibration signal.

Wei et al [7] have recently reported a real-time wheel defect monitoring system based on fibre Bragg grating sensors. The sensors measure the rail strain response during wheel and rail interaction and the frequency component alone reveals the quality of the interaction. The advantage of the fibre Bragg grating system is that it is not sensitive to electromagnetic interference. However, due to the fact the sensor has to be glued on to the rail its reliability and durability is still under investigation. It is apparent from the literature review that although work has been done to model and predict wheel/rail interaction in the frequency domain, no proper time-frequency analysis has yet been reported for the detection of wheel flats and rail surface defects despite the fact that time-frequency analysis method have been widely used for bearing, gearbox and engine fault identification [8-11]. In these examples time-frequency analysis has been shown to be a very effective tool for identifying the content of a signal in the frequency domain without losing its characteristics in the time domain. In many applications it is interesting to see the frequency content of a signal locally in time. That is, the way in which the signal parameters (frequency content etc.) evolve over time. Such signals are called non-stationary. For a non-stationary signal s(t), the standard Fourier Transform is not useful for

analysing the signal. Because information which is localised in time such as spikes and high frequency bursts cannot be detected from the standard Fourier Transform.

This paper presents an investigation into the use of time-frequency analysis of vibrations for the detection of railway wheel flats and rail surface defects. The sections of this paper are arranged as follows: in section 2, the basic time-frequency theories are given; in section 3, a simplified mathematic model is presented; in section 4, time-frequency vibration signal analysis for wheel and rail defects are presented and finally the conclusion are shown in section 5.

2. Time-frequency analysis techniques

The most commonly used time-frequency presentation is the Short-Time-Fourier-Transform (STFT), which originated from the well-known Fourier transform. Time-localisation can be achieved by first windowing the signal so as to cut off only a well localised slice of s(t) and then taking its Fourier Transform. The STFT of a signal s(t) can be defined as [12]:

$$STFT_s(t,\omega) = \int_{-\infty}^{\infty} h(\tau - t)s(t)e^{-j\omega t}\,dt \quad (1)$$

Where τ and ω denote the time of spectral localisation and Fourier frequency respectively, and h(τ-t) denotes a window function. However the STFT has some problems with dynamic signals due to its limitations of fixed window width.

Another well-known time-frequency representation is the Wigner-Ville distribution. The Wigner distribution was developed by Eugene Wigner in 1932 to study the problem of statistical equilibrium in quantum mechanics and was first introduced in signal analysis by the French scientist, Ville, 15 years later. It is commonly known in the signal processing community as the Wigner-Ville Transform [13].

Given a signal s(t), its Wigner-Ville transform is defined by

$$WV_s(t,\omega) = \int_{-\infty}^{\infty} s\,(t+\tau/2)s^*(t-\tau/2)e^{-j\omega\tau}\,d\tau \quad (2)$$

The Wigner-Ville transform $W_s(t,\omega)$ essentially amounts to considering the inner products of copies of $s(t+\tau)e^{-j\omega\tau}$ of the original signal shifted in time dominancy with the corresponding reversed copy $s(-t+\tau)e^{j\omega\tau}$. Simple geometrical considerations show that such a procedure provides insights into the time-frequency content of the signal. From the definition of equation (2) it can be seen that the calculation of Wigner-Ville transform requires infinite quantity of the signal, which is impossible in practice. One of practical methods is to add a window *h(τ)* to the signal. That leads to a new version of the Wigner-Ville transform called the pseudo-Wigner–Ville (PWV) representation and is as follows:

$$PWV_s(t,\omega) = \int_{-\infty}^{\infty} h(\tau)s\,(t+\tau/2)s^*(t-\tau/2)e^{-j\omega\tau}\,d\tau \quad (3)$$

However, there is a well-known drawback for using Wigner-Ville transform. The interferences or cross-terms exist between any two signals due to the fact the Wigner-Ville transform is a bilinear transform. For example, if a signal consists of signal 1 and signal 2, the Wigner-Ville transform of the signal is

$$PWV_s(t,\omega) = PWV_{s1}(t,\omega) + PWV_{s2}(t,\omega) + 2\mathcal{R}e(PWV_{s1,s2}(t,\omega)) \quad (4)$$

Where $PWV_{s1,s2}(t,\omega) = \int_{-\infty}^{\infty} h_1(\tau)s_1\,(t+\tau/2)\cdot h_2(\tau)s_2^*(t-\tau/2)e^{-j\omega\tau}\,d\tau$ is called the cross term Wigner-Ville transform of signal 1 and signal 2. The cross-term phenomenon is shown in Figure 1 by using an artificial signal created to demonstrate the effect. The artificial signal lasts for about 250ms, and consists of three signals added together in series (two signals with same frequency of 200Hz with one signal of 800 Hz in between). All three signals amplitudes are modulated using the Gaussian function. It can be seen that there are three cross-terms between any two of three signals in the Wigner-Ville transform. In order to get rid of the cross-term a smoothed pseudo Wigner-Ville transform or distribution (SPWVT or SPWVD) can be used. Figure 2 presents the smoothed pseudo Wigner-Ville transform for the same artificial signal. It demonstrates that the cross-terms are blanked out completely.

Finally another relatively new time-frequency analysis technique is the wavelet transform (WT). Fourier analysis consists of breaking up a signal into sine waves of various frequencies. Similarly, wavelet analysis is the breaking up of

a signal into shifted and scaled versions of the original (or mother) wavelet. One major advantage afforded by wavelets is the ability to perform local analysis. Because wavelets are localised in time and scale, wavelet coefficients are able to locally abrupt changes in smooth signals. Also the WT is good at extracting information from both time and frequency domains. However the WT is sensitive to noise.

For a signal s(t), the WT transform can be given as [13]

$$WT_s^{\psi}(\tau, x) = \Psi_s^{\psi}(\tau, x) = \frac{1}{\sqrt{|x|}} \int_{-\infty}^{\infty} s(t)\psi^*\left(t - \tau/x\right) dt \quad (5)$$

Where ψ(t-τ/x) is the mother wavelet with a dilation x and a translation τ which is used for localization in frequency and time.

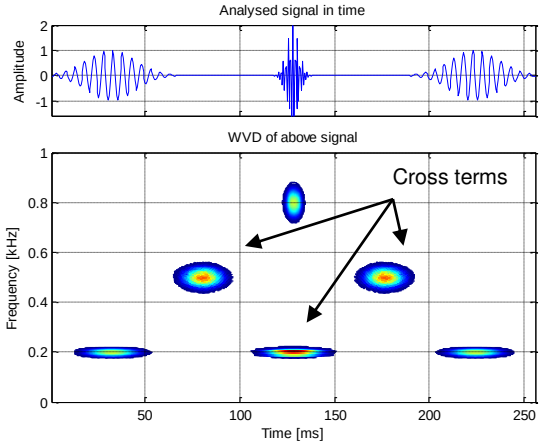

Figure 1 The Wigner-Ville representation of an artificial signal

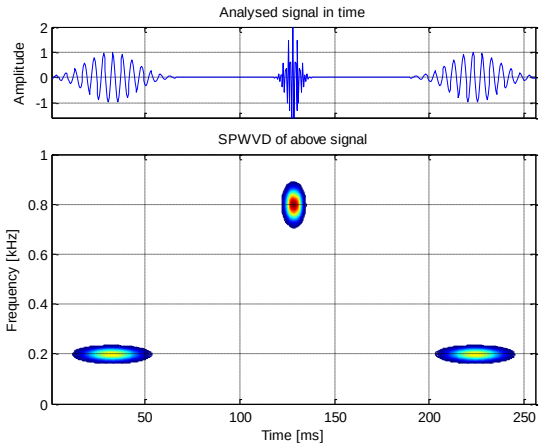

Figure 2 The smoothed Wigner-Ville representation of the artificial signal

3. Modelling of interactions between wheel and rail due to wheel or rail defects

Because the types of defect being considered in this work mainly result in changes to the vertical forces and accelerations experienced by the wheel and the rail. The other motions such as lateral, yaw, roll which are less influential on the targeted parameters, are not considered in the study. The simplified single wheel model on a roller rig is presented in Figure 3. From the standard matrix for Newton's second law:

$$[M]\{\ddot{Z}\} + [C]\{\dot{Z}\} + [K]\{Z\} = \{Q\} \quad (6)$$

The dynamic movement of the vehicle in vertical direction is given as follows [15]:

$$\begin{bmatrix} m_1 & 0 \\ 0 & m_2 \end{bmatrix}\begin{Bmatrix} \ddot{z}_1 \\ \ddot{z}_2 \end{Bmatrix} + \begin{bmatrix} c_1 + c_2 & -c_2 \\ -c_2 & c_2 \end{bmatrix}\begin{Bmatrix} \dot{z}_1 \\ \dot{z}_2 \end{Bmatrix} + \begin{bmatrix} k_1 + k_2 & -k_2 \\ -k_2 & k_2 \end{bmatrix}\begin{Bmatrix} z_1 \\ z_2 \end{Bmatrix} + \begin{Bmatrix} -m_1 g \\ -m_2 g + W \end{Bmatrix} = \begin{Bmatrix} c_1(\dot{z}_w + \dot{z}_r) + k_1(\dot{z}_w + \dot{z}_r) \\ 0 \end{Bmatrix} \quad (7)$$

Where $z_1(t)$ and $z_2(t)$ are the wheel and bogie displacements respectively, m_1—wheel mass, m_2—a quarter bogie mass, W—normal load, z_w and z_r are the wheel and rail vertical profile. For the Hertzian contact the damping coefficient c_1 is normally negligible [16]. The equation (7) can be simplified to:

$$\begin{bmatrix} m_1 & 0 \\ 0 & m_2 \end{bmatrix}\begin{Bmatrix} \ddot{z}_1 \\ \ddot{z}_2 \end{Bmatrix} + \begin{bmatrix} c_2 & -c_2 \\ -c_2 & c_2 \end{bmatrix}\begin{Bmatrix} \dot{z}_1 \\ \dot{z}_2 \end{Bmatrix} + \begin{bmatrix} k_1 + k_2 & -k_2 \\ -k_2 & k_2 \end{bmatrix}\begin{Bmatrix} z_1 \\ z_2 \end{Bmatrix} + \begin{Bmatrix} -m_1 g \\ -m_2 g + W \end{Bmatrix} = \begin{Bmatrix} k_1(z_w + z_r) \\ 0 \end{Bmatrix} \quad (8)$$

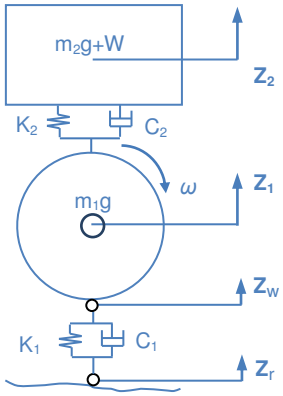

Figure 3 A simplified single wheel model

The combination of the wheel and rail profile ($z_w + z_r$) can be estimated by double integration of the vertical axle box acceleration measured using an accelerometer installed on the wheelset bearing housing. However due to the fact that all experiments were carried out on a roller rig, a high pass filter has to be used to remove the low frequency non-concentric rotation effect of roller. Figure 4 presents the measured axle box acceleration time history and the calculated velocity and displacement time histories without the high pass filter. It can be seen that the non-concentric rotation of roller accounts for significant vertical displacement. It completely masks the roller profile (Figure 4-c). In order to remove the non-concentric wheel and roller rotation effect, a 20 Hz Butterworth high pass filter was applied. For wheel speeds of 3.5km/h, 7km/h and 15km/h, the corresponding maximum wavelengths of the non-concentric displacements are 43.5mm, 87mm and 194mm which are significantly larger than the simulated roller surface defect (<3mm) and wheel flat (<2mm) on the experimental roller rig. The filtered result is given in Figure 5. It shows that the displacement caused by non-concentric rotation of the roller and wheel has been removed and the roughness of the combined wheel and roller profile is obtained (Figure 5-c). The big roller surface defect is clearly visible despite the wheel flat effect is pretty small. The estimated profile of wheel and roller is inputted in to equation 8 to simulate wheel vertical acceleration response of the system. The parameters used for the simulation are presented in Table 1. Three wheel speeds (3.5km/h, 7km/h and 15km/h) with the roller rig were applied. Despite the wheel linear speeds are different but the angular speed and the cyclic frequencies are the same for the roller rig and the full size vehicle. Hence the results obtained from the roller rig are applicable to the real situations. Figure 6 presents the comparison between the measured and the simulated wheel vertical acceleration results for the roller surface defect with wheel speed 3.5 km/h. It can be seen that a good agreement is achieved. A reasonable agreement between the measured and the simulated wheel vertical acceleration is also obtained for wheel speed 7km/h in Figure 7. However when the wheel speed reaches to 15km/h the disparity between the measured and simulated results gets bigger because the proposed simple model cannot represent the roller rig system properly in the high speed condition.

Table 1 The Experimental Roller Rig Parameters

Wheel mass M_1=6.35Kg	Wheel diameter, 0.2 m	Contact stiffness k_1=8.93x10^6 N/m	Suspension damping c_2= 2.67x10^3 N s/m
1/4 Bogie mass M_2=5.25Kg	Roller diameter, 0.38 m	Suspension stiffness k_2=36x10^3 N/m	Normal load = 140 N

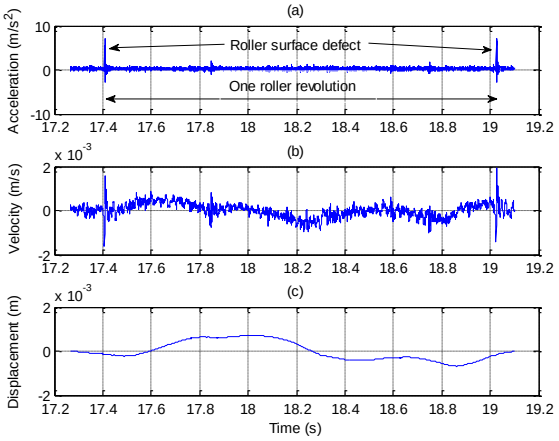

Figure 4 Axle box vertical acceleration (a), velocity (b) and the vertical displacement (c) with non-concentric rotation effect of wheel and roller (without high pass filter)

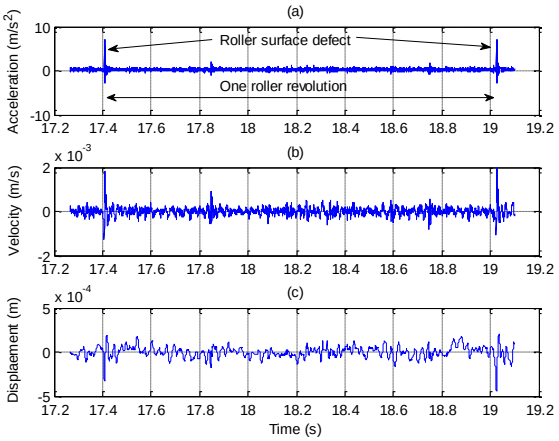

Figure 5 Axle box vertical acceleration (a), velocity (b) and the vertical displacement (c) of wheel and roller with the non-concentric rotation effect of the roller removed (with high pass filter)

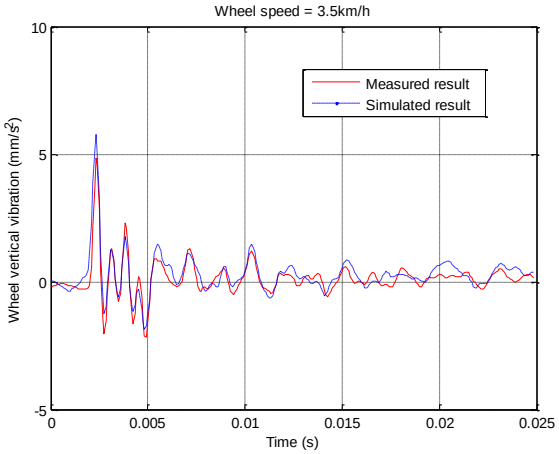

Figure 6 Comparison of measured and simulated wheel vertical accelerations (3.5km/h)

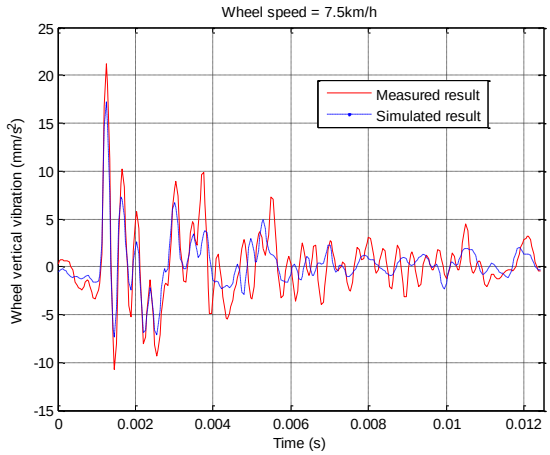

Figure 7 Comparison of measured and simulated wheel vertical accelerations (7km/h)

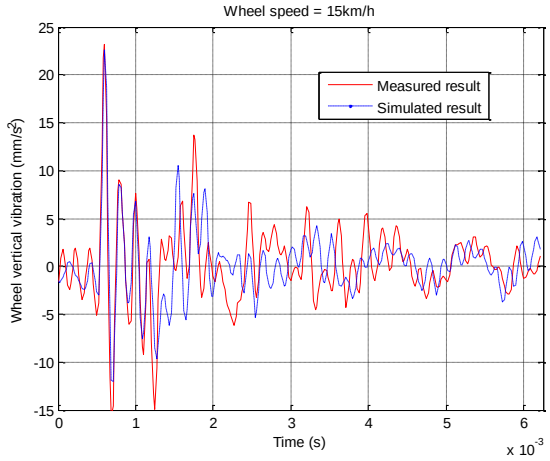

Figure 8 Comparison of measured and simulated wheel vertical accelerations (15km/h)

4. Time-frequency vibration signal analysis for wheel and rail defects

A series of experiments have been carried out on a roller test rig pictured in Figure 9. There are 5 accelerometers installed on each side of the roller rig; two on the wheel bearing housing (axle box, two on the roller bearing sets and one on the bogie. To obtain the sound signals an integrated microphone system was used. A reference signal obtained from a magnetic sensor was then used to synchronize time domain averaging of both the vibration and acoustic signals. The signals were sampled at 12 kHz. In order to get a better signal to noise ratio the seeded wheel flat size and rail surface defect are set proportionally larger than real wheel flat size (usually a 5-10 mm wide, 5-10 mm long and 0.5-2 mm deep surface fault on wheel and rail is often seen). A wheel flat that was 2 mm wide and 0.1 mm deep was produced on one wheel. A rail surface defect with a size of 2mm x3 mm and 0.2 mm deep was made on one of the four rollers. The typical impact pulses generated by wheel flats and roller surface defects are shown in Figure 10. Due to the fact that the defect size of roller is larger than wheel flat, the impact vibration caused by roller defect is bigger than the impact caused by wheel flat in this instance. Since the wheel diameter is slightly over half of the roller diameter, the wheel flat vibration and roller surface defect vibration are not completely synchronized. However this problem was solved by computer programming.

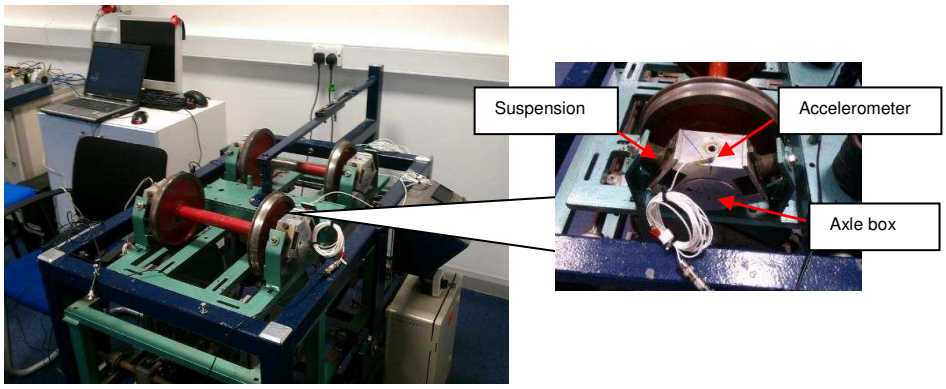

Figure 9 Roller test rig

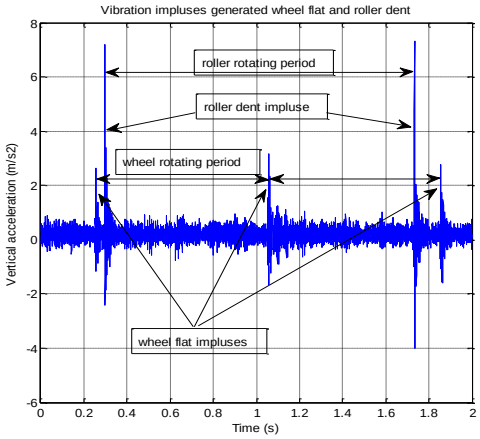

Figure 10 Typical impact pulses caused by wheel flat and roller defects

Because the impact vibration pulses generated by wheel flat and rail surface defects are similar in nature to vibrations seen at bearings, a number of traditional statistical indicators in time-domain used for ball bearing condition monitoring are also explored.

Figure 11 shows the values of crest factor, skewness, average maximum peak/cycle and average rms value/cycle of the vibration signals with and without wheel flats and under different wheel running speeds. It can be seen that all of the indicators show distinguishable values and trends under different wheel speed conditions for wheel vibrations with and without a wheel flat. A series of experiments has also been carried out to identify the effect of varying vehicle load. The vehicle load effect on the vibration impulse is presented in Figure 12. As expected the maximum vibration amplitude increases with increasing vehicle load. Figure 13 shows the wheelset vibration response coherence and its transfer function using a hammer test. It can be seen that the main wheelset natural frequency range is about 1300Hz-1500Hz and some low natural frequencies around 100-250Hz. The roller hammer test result is also given in Figure 14. It demonstrates the main roller natural frequency is much below the main wheel set natural frequency and mainly concentrates around 550Hz. There are some natural frequency overlaps for both wheel set and roller from 100Hz to 250 Hz.

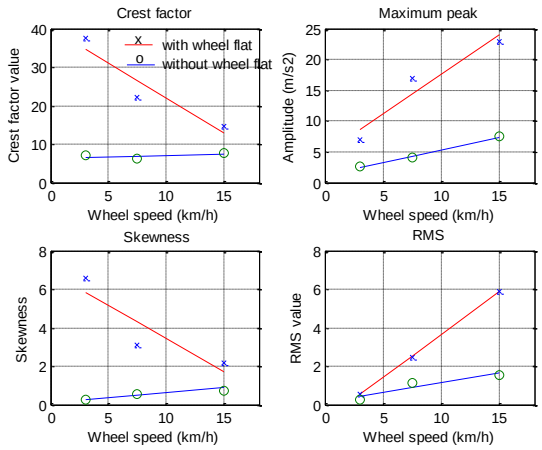

Figure 11 Crest factor, skewness, rms and peak values for a wheel with and without a wheel flat under different wheel speeds

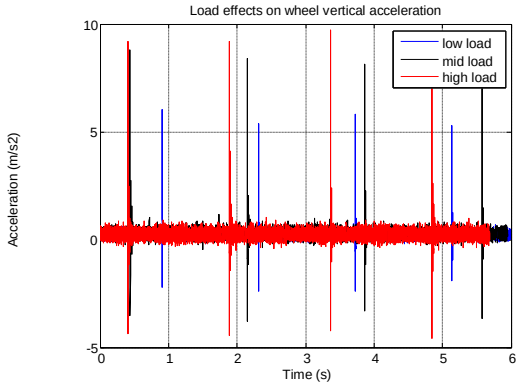

Figure 12 Vehicle load effects on wheel vertical acceleration

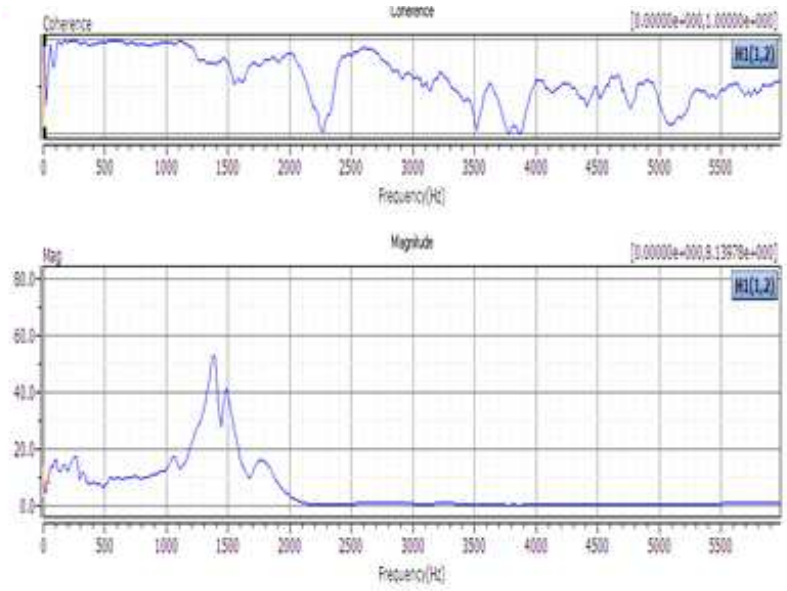

Figure 13 Coherence and transfer function of wheelset from the hammer test

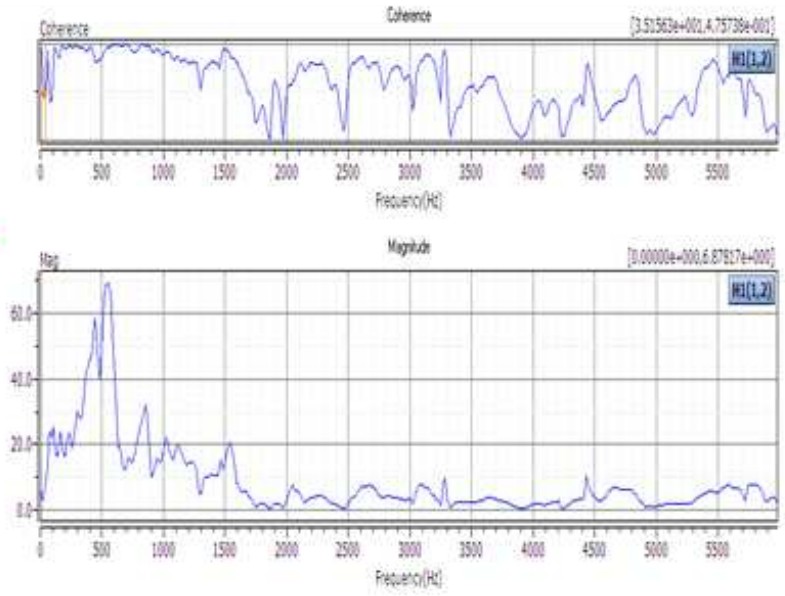

Figure 14 Coherence and transfer function of the roller from the hammer test

The three time-frequency techniques described in section 2, STFT, SPWVT, and WT were used to analyse the vibration and acoustic signal from the roller rig. Figure 15 displays one of the SPWVT results for wheel flat and roller surface defect conditions based on wheel vibration signals with a wheel speed of about 3.5 km/h. It is shown that the rail surface defect can excite the low natural frequency of the roller in the region of 250-550Hz but the wheel flat does not excite the wheelset natural frequency of 1300Hz. Due to the impact of the wheel flat being smaller, only low frequency modes around 250 Hz are visible for the wheel flat event. When the wheel speed increases to 7km/h (Figure 16), the SPWVD shows there are two strong frequency components at 250 Hz and 1300 Hz for the rail surface defect while the wheel flat made a similar impact as it did when the wheel speed was about 3.5km/h. When the wheel speed increases to 15km/h, the majority of the energy in the vibration signal from the roller surface defect is still concentrated at the frequency 250Hz and its harmonics at 1300Hz as illustrated in the SPWVT (Figure 17) but with a much stronger intensity. The main vibration frequency of the wheel flat impact is shifted to approximately 1300 Hz and is intensified.

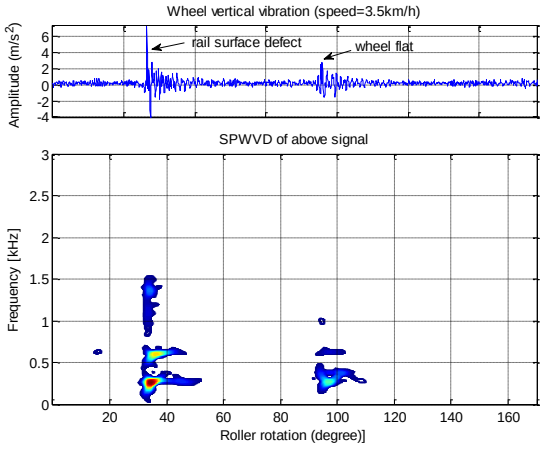

Figure 15 SPWVT of wheel vibration caused by roller surface defect and wheel flat (wheel speed=3.5km/h)

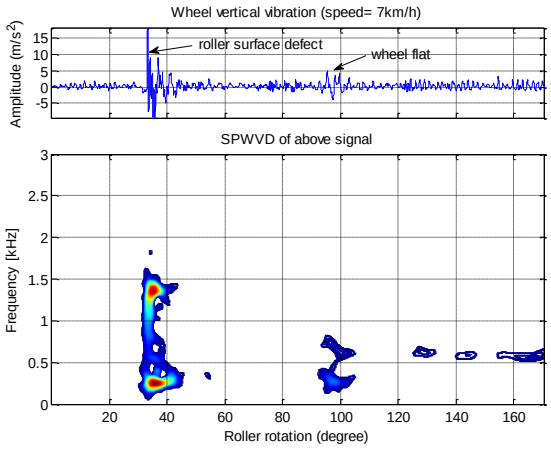

Figure 16 SPWVT of wheel vibration caused by roller surface defect and wheel flat (wheel speed=7km/h)

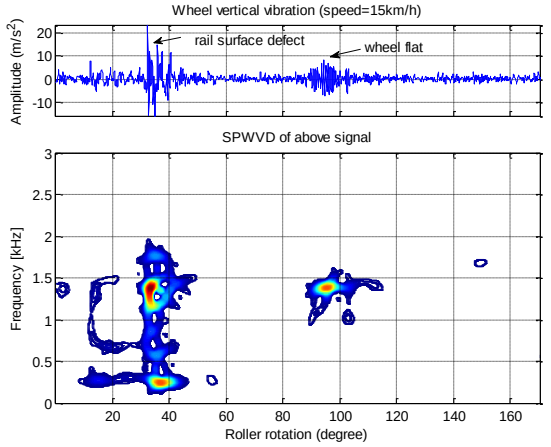

Figure 17 SPWVT of wheel vibration caused by roller surface defect and wheel flat (wheel speed=15km/h)

In order to compare the effects of different time-frequency techniques, the same vibration signals above are also analysed by STFT and WT. Figure 18-20 present the STFT results. It can be seen that the STFT can reveal similar information to the SPWVD but with slightly lower resolution. The WT representations are shown in Figures 21-23. Despite the slightly coarse results for the WT transform, for all three speeds WT presents much better localised vibration information in both time and frequency domain than SPWVT and STFT methods while the SPWVT processing demonstrates a better performance than STFT processing.

.

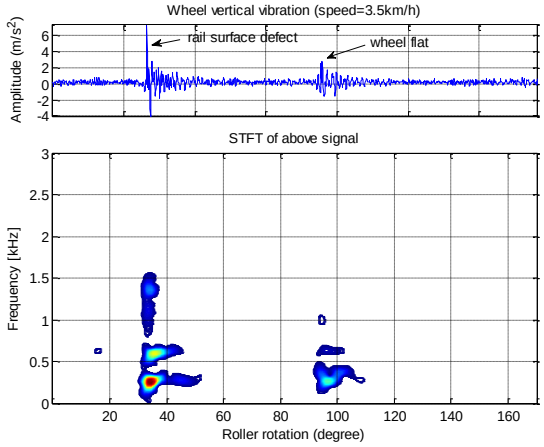

Figure 18 STFT of wheel vibration caused by roller surface defect and wheel flat (wheel speed=3.5km/h)

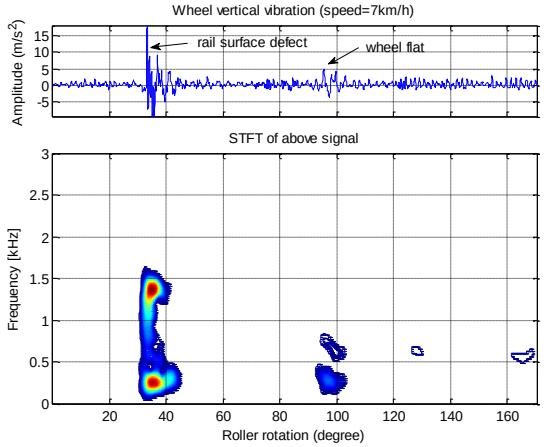

Figure 19 STFT of wheel vibration caused by roller surface defect and wheel flat (wheel speed=7km/h)

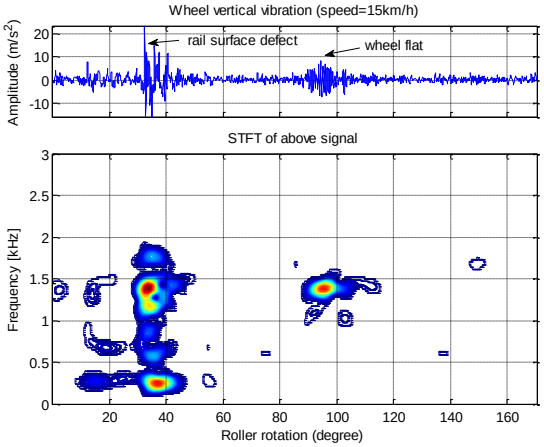

Figure 20 STFT of wheel vibration caused by roller surface defect and wheel flat (wheel speed=15km/h)

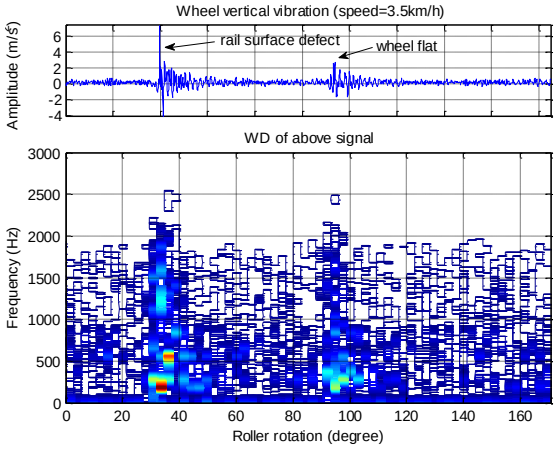

Figure 21 WT of wheel vibration caused by roller surface defect and wheel flat (wheel speed=3.5km/h)

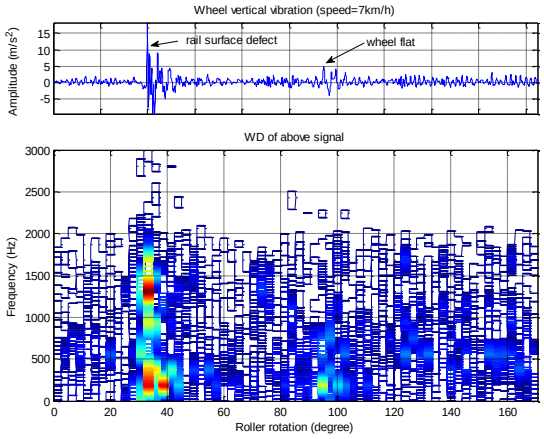

Figure 22 WT of wheel vibration caused by roller surface defect and wheel flat (wheel speed=7km/h)

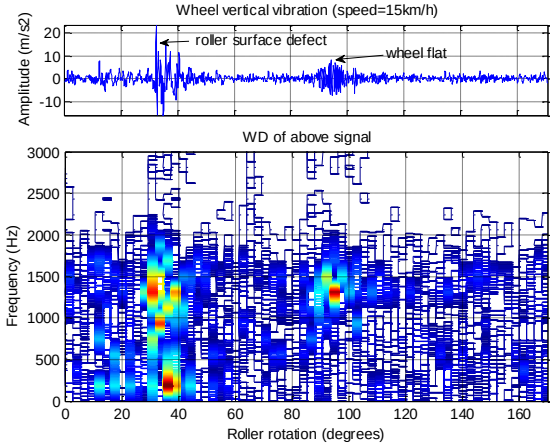

Figure 23 WT of wheel vibration caused by roller surface defect and wheel flat (wheel speed=15km/h)

The results of the measured acoustic and vibration signals (red colour for acoustic signal and blue colour for vibration signal) are presented in Figure 24. This shows that when the wheel is running at low speed (3km/h), the acoustic signal demonstrates good detection ability similar to the vibration signal for wheel flats and rail surface defects (Figure 24-a). With wheel speed increasing to 7.5km/h, the acoustic signal can still identify the impact noises generated by the wheel flats and rail surface defects (Figure 24-b). Further increasing the wheel speed to 15km/h, the acoustic signal is unable to pick up the signature of the wheel flats or the rail surface defects due to the roller rig background noise caused by

stronger sound resonant and reverberant mixing phenomenon (Figure 24-c). The SPWVT of acoustic signal is given in figures 25-27. Figure 25 presents the contour plot of SPWVT of acoustic signal for wheel speeding at 3 km/h. It can be seen that the dominant frequency is about 550 Hz for roller surface defects and 800Hz for wheel flats. At a higher wheel speed (7km/h), the SPWVT of the acoustic signal displays a few major frequency peaks at about 600Hz, 800Hz and 1400Hz for roller surface defects and 600Hz for wheel flats. It also shows a strong unidentified frequency component (750Hz) at locations of roller rotation 140 and 150 degrees. This may be caused by stronger roller rig sound reverberating and mixing effects. When the wheel speed reaches 15km/h, the acoustic signal is completely buried in very strong roller rig background noise (Figure 27). However the SPWVT does give a small indication at about 1100Hz at about 30^{o} roller rotation where the roller surface defect is expected.

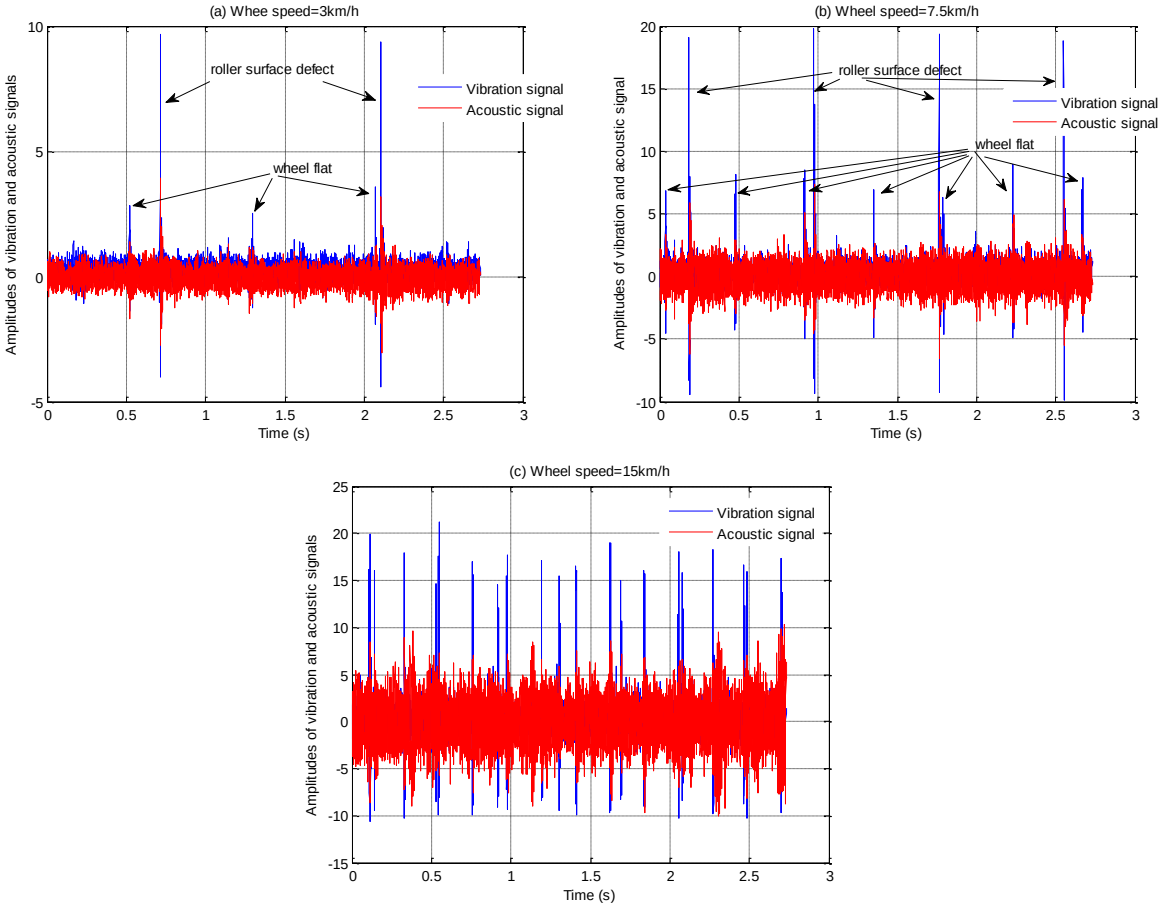

Figure 24 Comparison of measured vibration and acoustic signals under three different wheel running speeds

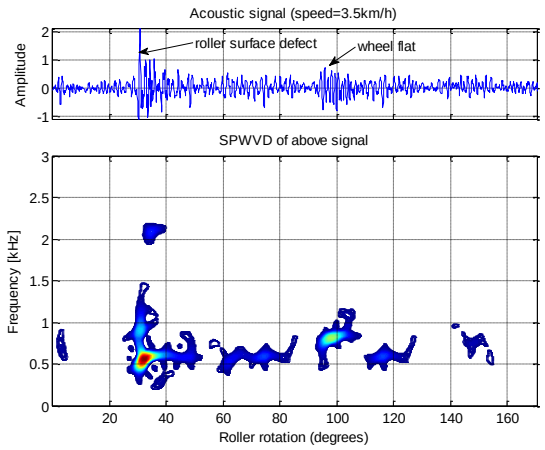

Figure 25 SPWVT of acoustic signal (wheel speed=3.5km/h)

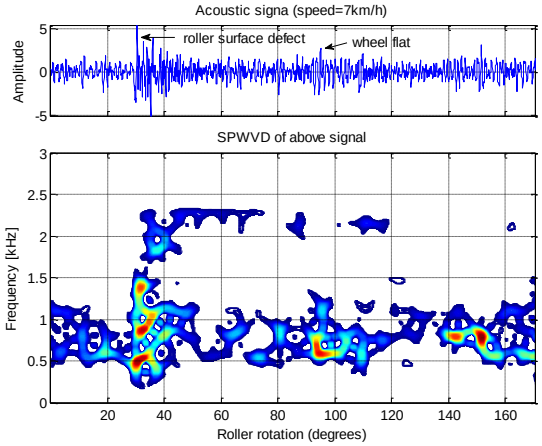

Figure 26 SPWVT of acoustic signal (wheel speed=7km/h)

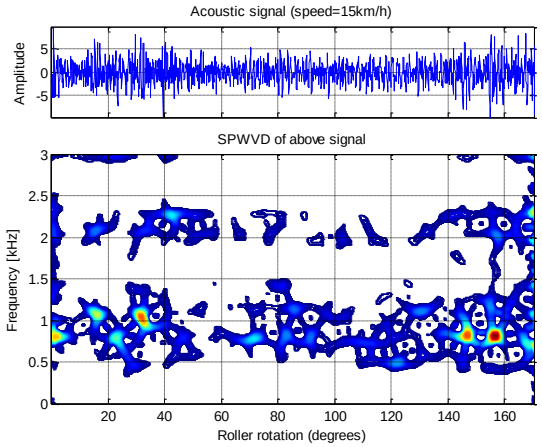

Figure 27 SPWVT of acoustic signal (wheel speed=15km/h)

5. Conclusions

In this research, a simplified mathematical model combined with a roller profile input estimated by the double integration of the axle box accelerometer on a roller rig, was used to simulate vibration caused by wheel flats and rail surface defects. A good agreement was achieved between simulated and measured accelerations results for low wheel speed (3.5 km/h). As the wheel speed got higher, the disparity between simulated and measured wheel accelerations becomes bigger as a result of the modelling limitation and some unknown nonlinear effects of the roller rig system. A series of experiments was carried out on a roller rig and the vibration and acoustic signals were analysed for rail surface defects and wheel flat faults by several time domain parameters including crest factor, skewness, rms and peak values, and time-frequency transforms. Both vibration and acoustic signals have been shown to have the ability to detect the faulty signal when the wheel speed is low but when the wheel speed is high, the acoustic signal cannot effectively determine the defects as that the original impact signal is completely buried by much stronger background reverberating acoustic noise. Although time domain parameters do reveal that big differences exist in vibration signals with and without wheel flats, there is a lack of useful frequency information. Time-frequency analysis shows that this drawback can be compensated easily. Three time-frequency analysis methods (STFT, SPWVT and WT) were used for rail surface and wheel flat defect identification. It was demonstrated that all three time-frequency methods can present proper time-frequency information for vibration generated wheel flat and rail surface defect. The SPWVT gives a better representation with a compromise of time and frequency resolutions while WT shows good localisations in both time and frequency dimensions.

References

[1] T.X. Wu and D.J. Thompson, “A hybrid model for the noise generation due to railway wheel flats”, Journal of Sound and Vibration, Vol. 251(1), pp115-139, 2002
[2] A. Pieringer and W. Kropp, “A fast time-domain model for wheel/rail interaction demonstrated for the case of impact forces caused by wheel flats”, Proceedings of Acoustics 08 Paris, pp2643-2648, Paris, 2008
[3] T. Mazilu, “A dynamic model for the impact between the wheel flat and rail”, U.P.B. Science Bulletin, series D Vol.69, No.2, pp45-58, 2007
[4] S.D. Newton and R.A. Clark, “An investigation into the dynamic effects on the rail of wheel flats on railway vehicles”, Journal of Mechanical Engineering Science, Vol. 21, No.3, pp253-269, 1999
[5] V. Belotti, F. Crenna, R. C. Michelini, and G. B. Rossi, “Wheel-flat diagnostic tool via wavelet transform” Mechanical Systems and Signal Processing Vol. 20, No.2, pp1953-1966, 2006
[6] S. Jia and M. Dhanasekar, “Detection of rail wheel flat using wavelet approaches”, Structural Health Monitoring, Vol. 6, No.2, pp121-131, 2007
[7] C. Wei, Q. Xin, W.H. Chong, “Real-time train wheel condition monitoring by fiber bragg grating sensors”, International Journal of Distributed Sensor Networks, Vol.4, pp127-134, 2012
[8] V.V. Polyshchuk, F. K. Choy and M. J. Braun, “Gear fault detection with Time-frequency based parameter NP4”, International Journal of Rotating Machinery, Vol.8, No. 1, pp57-70, 2002
[9] C. Wang, Y. Zhang and Z. Zhong, “Fault diagnosis for diesel valve trains based on time–frequency images”, Mechanical system and signal processing, Vol. 22, No.3, pp1981-1993, 2008
[10] N., Baydar and A. Ball, “A comparative study of acoustic and vibration signals in detection of gear failure using Wigner-Ville distribution”, Mechanical Systems and Signal Processing, Vol.15, pp1091-1107, 2001
[11] G. Dong and J. Chen, “Noise resistant time frequency analysis and application in fault diagnosis of rolling element bearings”, Mechanical System and Signal Processing, Vol.23, No.11, pp212-236, 2012
[12] F. Hlawatsch and F. Auger, “Time-Frequency Analysis”, John Wiley & Sons Inc, Hoboken, USA 2005
[13] S. Qian, Introduction to time-frequency and wavelet transforms, Prentice Hall, London, 2002
[14] J. Real, P. Salvador, L. Montalban and M. Bueno, “Determination of rail vertical profile through inertial methods”, Proceedings of IMechE, part F, Rail and Rapid Transit, Vol. 225, pp360-372, 2011
[15] Y. Q. Sun and M. Dhanasekar, “A dynamic model for the vertical interaction of the rail and wagon system”, International Journal of Solids and Structures, Vol. 39, No.3, pp1337-1359, 2002